Journal of Nanophotonics

Nanophotonics.SPIEDigitalLibrary.org

Fast and reliable approach to calculate energy levels in semiconductor nanostructures

François Thierry
Judikaël Le Rouzo
François Flory
Gérard Berginc
Ludovic Escoubas

SPIE.

Fast and reliable approach to calculate energy levels in semiconductor nanostructures

François Thierry,[a,*] Judikaël Le Rouzo,[a] François Flory,[a,b] Gérard Berginc,[c] and Ludovic Escoubas[a]

[a]Aix-Marseille Université, Institut Matériaux Microélectronique Nanosciences de Provence-IM2NP, CNRS-UMR 7334, Domaine Universitaire de Saint-Jérôme, Service 231, 13397 Marseille, France

[b]Ecole Centrale Marseille, 38 rue Joliot Curie, 13451 Marseille, France

[c]THALES Optronique SA, 2 Avenue Gay Lussac, 78990 Elancourt, France

Abstract. We propose a method under the effective mass approximation with an original formulation that applies to quantum wells, circular quantum wires, and spherical quantum dots of arbitrary materials with sizes as small as 1 nm. Hundreds of structures are resolved on the second scale on a laptop, allowing for optimization procedures. We demonstrate its capability by confronting bandgap calculations with exhaustive literature data for CdS, CdSe, PbS, and PbSe nanoparticles. Our approach includes a correction of the mass to address the nonparabolicity of the band structure. The correction gives an accuracy comparable to more demanding calculation methods, such as eight-band k · p, tight-binding, or even semiempirical pseudopotential methods. The effect of the correction is shown on the intrasubband optical properties of InGaAs/AlGaAs coupled quantum wells. [DOI: 10.1117/1.JNP.9.093080]

Keywords: effective mass approximation; nonparabolicity; nanostructures; CdS; CdSe; PbS; PbSe; coupled quantum wells.

Paper 14117P received Oct. 10, 2014; accepted for publication Jan. 27, 2015; published online Mar. 6, 2015.

1 Introduction

Nanostructures are used in optoelectronic applications because their optical and electrical properties can be tuned by changing the materials, composition,[1] or geometries.[2] Recent progress in formulation and modeling have led to a considerable growth of their use in various applications.[3] When designing devices, in order to evaluate which association and form of materials will give the expected behavior, accurate numerical studies have to be performed. In addition, those calculations have to be fast to perform optimization routines.

Due to confinement effects which change the electronic properties, quantum structures exhibit behaviors different from that of the bulk.[3] The size dependence of the energy levels has brought increasing interest for their use in optoelectronic devices, especially in photovoltaic solar cells.[4] Simulations improve our understanding of the physics in nanosystems, potentially allowing to perform systems optimization through numerical experiment without delays or costs. But fast techniques lack accuracy and more precise ones are too computationally intensive to be used in optimization. The optical and electrical responses of nanoscaled optoelectronic materials are directly related to the electronic properties. The precise evaluation of the confined energy levels is crucial. Speed and accuracy depend on the numerical method employed.

Numerous techniques are available to calculate energy levels in nanostructures.[5] They cover a wide range of purposes based on the scale under study. The most simple ones that are based on the particle-in-a-box (PIB) model,[6] like the effective mass approximation (EMA)[7] or quantum transfer matrix methods,[8] are fast and give the general deviation from the bulk theory. They are

*Address all correspondence to: François Thierry, E-mail: francois.thierry@im2np.fr

1934-2608/2015/$25.00

suitable to study structures ranging from tenths of nanometers to several micrometers. More precise approaches based on multiband methods, such as tight-binding[9] or k · p methods,[10] allow a more precise evaluation of the electronic properties in the range of a few Angström to hundreds of nanometers. It should be noted that the EMA is a one-band k · p method. Atomistic and *ab initio* calculations, such as pseudopotential methods[11] and density functional theories,[12] are exact, but they are limited to the study of a few thousands of atoms due to hardware and time limitations.

We present and justify the choice of a fast EMA method with a new formulation to enhance its accuracy, stability, and usability. Typically, calculations on 1000 points take 0.2 s on a laptop, allowing us to study and to optimize solar cells incorporating components at the nano-scale. The accuracy of the approach is further improved by correcting the effective mass with an energy dependence. Furthermore, the core equation is reported under a general form which can be applied directly to all three dimensions of confinement for quantum structures. Our method needs only a few inputs to calculate. The necessary inputs are the effective mass of the charges, the bulk bandgap, and the electronic affinity. The effective masses are sufficient to calculate the energy levels relative to the bottom of the potential applied. The bulk bandgaps give the absolute values of the energies and allow the nonparabolicity correction. The electronic affinity places the potential in comparison to the vacuum level.

In this study, we first introduce the main concepts behind the effective mass approach. We explain why the nonparabolicity of the band structure is the main cause of inaccuracies. We then present our method and emphasize the accuracy of the current approach by comparing it to extensive published results of both calculated and measured bandgaps of CdS, CdSe, PbS, and PbSe quantum dots (QDs). We consider a coupled InGaAs/AlGaAs quantum wells example to explicit the necessity to address the nonparabolicity and to show the improvement given by its proposed correction. We conclude with the use of the results, the interest of the method, and the remaining points of improvement of the model.

2 Numerical Model

2.1 *Effective Mass Approximation, Theory and Limit*

We consider a single charge of mass m^* in a structure in steady state. We calculate the electronic properties using the time-independent Schrödinger equation. The charge has a particular kinetic energy, which is impacted by interactions between other charges within the solid. The effective mass approximation allows one to represent those interactions directly in the mass. The dispersion relation for a free electron gas gives us the analytic PIB relation to determine the energy levels available to a single charge in a solid.

$$E = \frac{\hbar^2 k^2}{2\ m^*}. \tag{1}$$

Behind this known equation [6] lies a parabola expression. In fact, the PIB model approximates the band structure around the gap to a parabola from which the curvature radius will condition the effective mass and energy levels dispersion. The curvature at the extrema of this parabolic dispersion curve is expressed in a second derivative. A large curvature implies a large second derivative or a small radius of curvature that will lead to a small effective mass and vice versa.

Actual band structures show that the approximation by a parabolic shape is valid only upon a small energetic domain near the band's edge. This is the main limit of the effective mass approximation and the main source of errors. It limits the resolution of the high-energy levels that are increasingly inaccurate the further away they are from the band edge. This is due to the fact that the radius of curvature of the approximate shape is not constant but increases with the energy. This can be taken into account by an effective mass that increases accordingly with the energy. That is the reason why it is difficult to resolve the properties of low-bandgap materials under EMA.[13] It is due to the domain of validity of the parabolic assumption that will be small in comparison to the actual band structure. Furthermore, the confinement effect that increases the energy levels separation will lead to another limit of resolution for small sizes.

2.2 *Numerical Approach*

Now that we have seen some of the phenomenological aspects of the nonparabolicity limitation when using EMA, we describe our method. The most common approach to solve the time-independent Schrödinger equation is to use finite difference and calculate the eigenvalues and eigenfunctions of a tridiagonal matrix.[14] Less employed in the semiconductor community, a faster technique[15] when using finite difference is the shooting technique.[16] To avoid numerical instabilities due to abrupt changes at the interface between materials, we work in the context of slowly varying the envelope function of the wavefunction. Furthermore, special attention has been payed to the ordering of the operators inside the Hamiltonian.[17,18]

We use a shooting method implemented from Harrison's book.[19] We further improved the speed and stability by reformulating the shooting equation in a set of two coupled ones. We followed a methodology presented for III/V quantum wells.[20] The speed is increased by a factor of six thanks to the reduced number of floating point operations that also limits numerical imprecisions. We propose an original general formulation that can be applied to two-dimensional, one-dimensional (1-D), and zero-dimensional (0-D) quantum structures. To regroup the three dimensions in a single equation, the position is represented in scalar, cylindrical, and spherical coordinates for quantum wells, wires, and dots, respectively. We obtain the following coupled shooting equations, where the energy level $E_{n,l}$ of a particular state corresponding to primary quantum number n and angular quantum number l ($l = 0$ in quantum wells) can be found by solving for E of the system of Eqs. (2) and (3). The boundary conditions resulting from the continuity at the interfaces condition for which we have to solve are $\psi_{n,l}(\pm\infty) = 0$ and $\partial\psi_{n,l}(\pm\infty)/\partial r = 0$:

$$\psi_{n,l}(r + dr) = \frac{rdrm^*(r)}{r + (N-1)m^*(r)}\tilde{\psi}_{n,l}(r) + \psi_{n,l}(r), \tag{2}$$

$$\tilde{\psi}_{n,l}(r + dr) = \frac{2dr}{\hbar^2}\left[V(r) + \frac{\hbar^2 l(l+N-2)}{2r^2 m^*(r)} - E\right]\psi_{n,l}(r) + \tilde{\psi}_{n,l}(r). \tag{3}$$

$N = 3 - X$ is the dimensionality of an X dimensional quantum structure ($X = 0$, 1, or 2), r is the position in meters expressed in the correct coordinate system, $\psi_{n,l}$ is the radial part of the envelope of the wavefunction, m^* is the effective mass in kilograms, and V is the potential applied on the position r in electron volts. The first points of the shooting procedure are $\psi_{n,l}(0) = 0$ and $\tilde{\psi}_{n,l}(0) = 1$.

For 1-D and 0-D structures, the mathematical development exploits the symmetry of cylindrical and spherical geometries. We start the evaluation of the energy levels from the middle of the structures with $\psi_{n,l}(0) = 1$ and $\tilde{\psi}_{n,l}(0) = 1$ as starting values. But, as the EMA derives from the PIB model, ΔE should also linearly depend on S/D^2, the inverse of the square diameter or length.[21] The slopes S are 1.0,[22] 1.17,[23] and 2.0[24] for wells, wires, and dots. respectively. We verified that we retrieve the same results between the calculations starting from the middle of the structure and the ones starting at one end for which we multiplied the corresponding energy by the appropriate slope. This allows the study of laterally coupled quantum structures, the calculation running along the axis that goes to all the centers of symmetry.

The implementation of this method is straightforward, allowing the quick evaluation of the electronic properties of most nanostructures, and should be of interest to many scientific studies covering a wide spectrum of applications. Our code is written in Python except for the core equations that are implemented in Cython for speed. The wavefunction envelopes calculated with this method have to be normalized according to $\psi(r) \rightarrow \psi(r)/\sqrt{\int \psi^2(r)\mathrm{d}r}$ to be quantitatively compared within models like the electrostatic dipole approximation that serves to determine the optical properties of nanostructures.

2.3 *Nonparabolicity Correction*

The nonparabolicity correction[19] applies a parabolic increase to the effective mass that is conditioned by the energy difference from the band edge normalized by the amplitude of the bandgap to scale the effect. The value of the effective mass at each point of the structure is corrected according to the value of the potential V and bulk bandgap E_g applied at their coordinate r:

$$m^*(r, E_{n,l}) = m^*(r)\left\{1 + \left[1 - \frac{m^*(r)}{m_0}\right]^2 \frac{E - V(r)}{E_g(r)}\right\}. \quad (4)$$

It should be noted that $E_g(r)$ is size-dependent. The bandgap—and with it the error—increases with small sizes due to confinement effects. In our approach, we use the bulk values only to calculate the first levels in the conduction and valence bands. They present the smallest deviations due to nonparabolicity, reassuring the extraction of the effective bandgap of a particular size. We then reuse the calculated value of the gap to apply the nonparabolicity correction upon higher levels. The study of the bandgap will, therefore, yield information about the validity of the method and can be used to study the small size limit in particular.

3 Results and Discussion

3.1 *Model Validation*

We study the limits of the method through the evaluation of the bandgap of three-dimensional QDs because they present the largest confinement effects. The large variations due to size confinement highlights the capabilities of our approach. The bandgap also presents the smallest deviations due to the nonparabolicity effect. We present our results against semiconductors of different bulk bandgaps to show the accuracy of the method and the capability to resolve low-bandgap materials. The chosen materials are CdS, CdSe, PbS, and PbSe, in association with other materials; they present interest for applications like QD solar cells. The input material properties are listed in Table 1.

We confront it against the Brus equation [24] that corrects the PIB model through a screening term that describes electrostatic forces. The Brus equation is often reported as a first approximation in publications concerning QDs because it extends the validity range of the PIB model while keeping the speed of resolution and retaining the simplicity. This equation is valid only for spherical geometries. Kayanuma further improved this formulation by accounting for the spatial correlation between the charges with the effective Rydberg energy.[30]

We also corroborate our results with published data from the literature. Those data are the experimental positions of the first absorption peaks and their corresponding calculation with more accurate but more computationally demanding methods, such as the ones mentioned in Sec. 1. The absorption data are fitted by a sizing curve of the form:

Table 1 Values of the bulk bandgap E_g, effective masses for electrons m_e^* and holes m_h^*, and electronic affinity χ_A used in the calculations.

	E_g (eV)	m_e^* (m_0)	m_h^* (m_0)	χ_A (eV)
CdS	2.53 (Ref. 13)	0.18 (Ref. 13)	0.53 (Ref. 13)	3.6 (Ref. 25)
CdSe	1.75 (Ref. 13)	0.13 (Ref. 13)	0.3 (Ref. 13)	3.93 (Ref. 26)
PbS	0.48 (Ref. 27)	0.085 (Ref. 13)	0.085 (Ref. 13)	4.6 (Ref. 28)
PbSe	0.29 (Ref. 29)	0.047 (Ref. 29)	0.041 (Ref. 29)	4.7 (Ref. 28)

$$E_g(D) = E_{g,\text{bulk}} + \frac{1}{aD^2 + bD + c}. \tag{5}$$

We model the QDs with finite potential as nanospheres of a certain dimension comprised between vacuum domains of same sizes. The spatial resolution is fixed to $dr = 0.01$ nm for all the calculations presented.

We fixed the band offsets between the materials and the vacuum. This allows the results to become more independent of the matrix and, thus, allows the comparison of data from different sources. We use the values of the electronic affinity χ_A from the literature (Table 1) as a band offset in the conduction band. In the valence band, we use $\chi_A + E_g$. This allows the method to be more accurate and to compare the calculation with arbitrary absorption data.

We start our study with CdSe (Fig. 1), which has a large bandgap. There are numerous literature data on bandgap size-confinement.[31–38] We find that the Brus formulation diverges for sizes <8 nm in diameter. Our EMA results are following those of the sizing curve to a diameter of ~1.5 nm. We retrieve the results of the semiempirical pseudopotential method (SEPM).[31] As expected, because the bandgap concerns band edges, the improvement over parabolic calculations (dashes) are weak.

We find a similar agreement for PbSe QDs (Fig. 2). Our calculations tightly follow the experimental results[39–47] until a size of 1 nm. The Brus equation shows its limits and overestimates the bandgap for the whole range of sizes considered. We are in agreement with the results of SEPM calculations to a size of 2.5 nm. We also retrieve the results (crosses) of a bandgap extraction procedure that is based on self-consistent optimization between absorption measurements and sizes that are measured by a transmission electron microscope.[48] The nonparabolicity effects are small for the charge levels under consideration.

The insets in the figures validate the positions of the band edges calculated using our formulation that are in close agreement with experimental measurements obtained by cyclic voltammetry. This approach has been conducted on various QDs for solar cells.

The comparison of our results with the fit of the experimental values [Eq. (5)] allows us to estimate the accuracy of our method in comparison with other parameters, such as bulk bandgaps and sizes. Figure 3 presents the deviation in electron volts between our results with the correction and the sizing curve for the semiconductors of this study. We consider 100 sizes ranging from 0.5 to 16 nm. The method presents little deviation (<50 meV) with the experimental fit to a size of ~3 nm, where the lack or discrepancy of experimental data along with strong energetic changes due to confinement make the comparison hazardous. This test depends heavily on the quality of

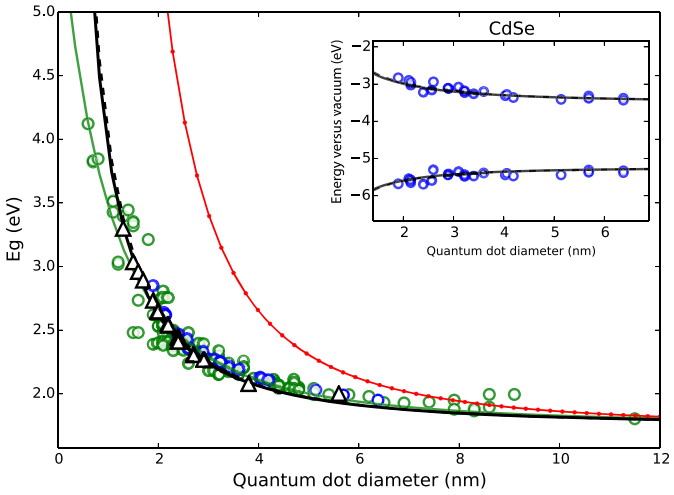

Fig. 1 Calculation of the bandgap of CdSe nanospheres with (solid line) and without (dashed line) the nonparabolicity correction. Comparison with semiempirical pseudopotential calculations[31] (triangles) and experimental data[31–38] (circles) from the literature. The results with Brus equation (red-dotted line) and the sizing curve (green line) are also drawn. The inset shows the results in comparison to conduction and valence band edges measured by cyclic voltammetry.[31,38]

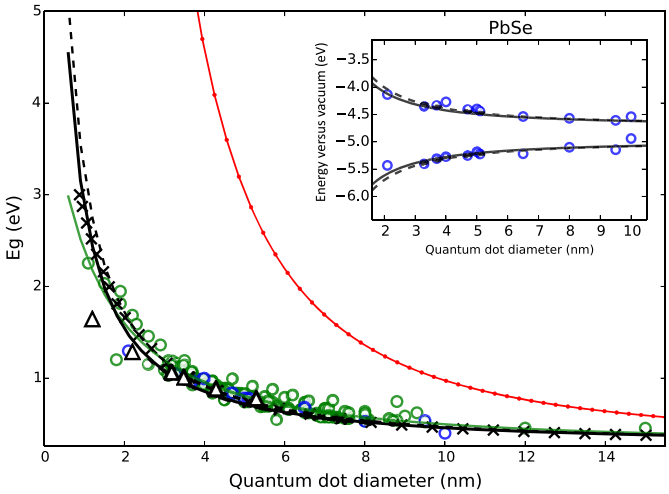

Fig. 2 Calculation of the bandgap of PbSe nanospheres with (solid line) and without (dashed line) the nonparabolicity correction. Comparison with semiempirical pseudopotential calculations[31] (triangles) and experimental data[39–47] (circles) from the literature. The results with Brus equation (red-dotted line) and the sizing curve (green line) are also drawn. The inset shows the results in comparison to conduction and valence band edges measured by cyclic voltammetry.[49,50]

the fit; the more the data points, the better is the fit. The results for CdS present a higher deviation. This is due to the lack of data points that give a less accurate fit. Nonetheless, we find that the mean deviation under 100 meV is ∼15 meV, which corresponds to a shift of ∼5 nm when compared to experimental spectra from optical measurements. It should also be emphasized that the fitted experimental data come from different sources whose samples are in different host materials, prepared with different methods, caped with different ligands.[51] All those aspects affect the electronic affinity, the confinement potential, and, thus, the energy levels, inducing additional deviations that are the main reasons for the dispersion of the data around the fit. A better comparison with experimental data would need a more careful study on those aspects. Moreover, this figure also highlights the imprecision of the bandgap measurements for QDs with sizes <2 nm. We also observe the deterioration of the resolution and the

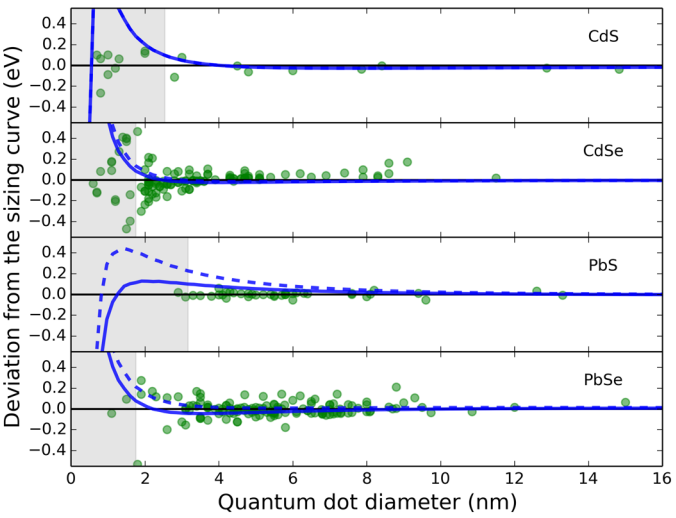

Fig. 3 Test of the performance of the method with (blue lines) and without (dashes) the nonparabolicity correction to determine the confined bandgap of four semiconductors through the deviation from the sizing curve of Eq. (5). Deviations over 100 meV are indicated by the gray area. The position of each literature data point in comparison to the fit is also reported (green points).

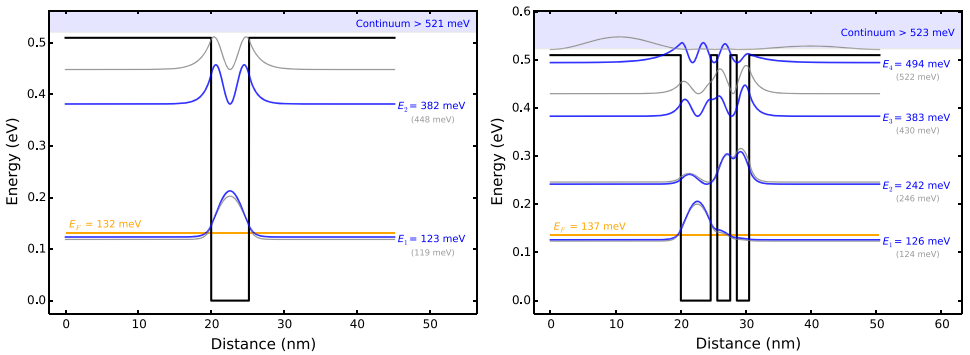

Fig. 4 Calculations of the confined energy levels in the conduction band of $Ga_{0.47}In_{0.53}As$/$Ga_{0.47}In_{0.53}As$ single-well and triple-well structures with (thick blue lines) and without (thin gray lines) the nonparabolicity correction of Eq. (4). We retrieve results of eight-band k · p calculations and experimental intersubband absorption.[52] The Fermi level is also reported.

improvement given by the nonparabolicity correction for decreasingly low-bandgap materials. We stress that the nonparabolicity correction should not be discarded when studying higher energy levels. To highlight this point, we compare our calculations to some results in the literature, where the nonparabolicity effects have been studied.

3.2 *Example Application: Coupled Quantum Wells*

We show the necessity of taking the nonparabolicity correction into account through the example of coupled $Ga_{0.47}In_{0.53}As$ quantum wells in $Al_{0.48}In_{0.52}As$ barriers (Fig. 4) by comparing the results of our calculations with those calculated and measured by Sirtori et al.[52] This example was also used by nextnano GmbH[53] to show the advantage and proper implementation of their 8×8 k · p method over their previous EMA model. Moreover, this article presents interest for quantum cascade lasers. We retrieve the eight-band k · p energies of the publication with a precision under 1 meV. They also realized those structures experimentally and the results are in close agreement (2 meV or less) with the position of the peaks of the intersubband absorption spectra that correspond to the transitions between the levels.

The material parameters are $m_e^* = 0.043m_0$ and $E_g = 0.69$ eV for the $Ga_{0.47}In_{0.53}As$ wells and $m_e^* = 0.072m_0$ and $E_g = 1.22$ eV for the $Al_{0.48}In_{0.52}As$ barriers. The conduction band offset between the two materials is $\Delta V_e = 0.51$ eV. The largest well is n-doped with silicon in order for the Fermi energy E^F to lie just above the first state. The doping induces a sheet density of $\rho_S = 3.2 \times 10^{11}$ cm^{-2}.

We can see from Fig. 4 that the nonparabolicity effect is negligible for the first states, but as soon as the energy is on the order of half the potential height, it induces a discrepancy that will shift all the transitions associated with this level. Furthermore, we notice that, for the triple-well structure without the correction, the fourth confined level will be in the continuum resulting in a missing peak on the intersubband absorption spectrum. As the same phenomenon applies to the holes, the impact of this discrepancy will be roughly doubled in interband processes. This is why an appropriate nonparabolicity correction should be used when using the results of the electronic calculations with EMA models to simulate the optical response of nanostructures.

4 Conclusion

The EMA method presented in this paper can be applied to quantum wells, wires, and dots structures. Our formulation is simple yet accurate, easy to implement, and can be performed in few microseconds on a particular structure. For the semiconductors under consideration, our method requires fewer inputs, while retaining a similar accuracy to other methods, such as the k · p, tight-binding, or pseudopotential methods. We highlighted the limiting cases of narrow bandgap materials or energies that are far away from the band edges, which we explained with phenomenological considerations. Those limitations have been corrected by transforming

the effective mass to be energy-dependent in order to account for the nonparabolicity of the band structure. We provide examples of bandgap calculations obtained with our approach, which compare well with published work on CdS, CdSe, PbS, and PbSe QDs. We have shown the improvement given by the nonparabolicity correction for levels that are higher than half of the confinement potential with the example of GaInAs/AlInAs coupled quantum wells. We have tested our method on several semiconductors to conclude that the method should yield accurate results on a wide range of materials given the appropriate input parameters. Further work about the determination of electronic and optical properties of QD materials solar cells using our technique will be carried out.

References

1. M. Jaros, "Electronic properties of semiconductor alloy systems," *Rep. Prog. Phys.* **48**(8), 1091 (1985).
2. Y. Kayanuma, "Wannier excitons in low-dimensional microstructures: shape dependence of the quantum size effect," *Phys. Rev. B* **44**, 13085–13088 (1991).
3. F. Flory, L. Escoubas, and G. Berginc, "Optical properties of nanostructured materials: a review," *J. Nanophotonics* **5**(1), 052502 (2011).
4. A. J. Nozik, "Nanoscience and nanostructures for photovoltaics and solar fuels," *Nano Lett.* **10**(8), 2735–2741 (2010).
5. Y. Saad, J. R. Chelikowsky, and S. M. Shontz, "Numerical methods for electronic structure calculations of materials," *SIAM Rev.* **52**(1), 3–54 (2010).
6. C. Kittel, *Physique de l'État Solide: Cours et Problèmes*, Sciences sup, Dunod (2005).
7. L. J. Sham and M. Nakayama, "Effective-mass approximation in the presence of an interface," *Phys. Rev. B* **20**(2), 734–747 (1979).
8. B. Jonsson and S. T. Eng, "Solving the Schrödinger equation in arbitrary quantum-well potential profiles using the transfer matrix method," *IEEE J. Quantum Electron.* **26**(11), 2025–2035 (1990).
9. C. M. Goringe, D. R. Bowler, and E. Hernández, "Tight-binding modelling of materials," *Rep. Prog. Phys.* **60**(12), 1447–1512 (1997).
10. L. Voon and M. Willatzen, *The k·p Method: Electronic Properties of Semiconductors*, Springer, Berlin, Heidelberg (2009).
11. D. Andrae et al., "Energy-adjusted ab initio pseudopotentials for the second and third row transition elements," *Theor. Chim. Acta* **77**(2), 123–141 (1990).
12. P. Geerlings, F. De Proft, and W. Langenaeker, "Conceptual density functional theory," *Chem. Rev.* **103**(5), 1793–1873 (2003).
13. G. Pellegrini, G. Mattei, and P. Mazzoldi, "Finite depth square well model: applicability and limitations," *J. Appl. Phys.* **97**(7), 073706 (2005)
14. P. J. Cooney, E. P. Kanter, and Z. Vager, "Convenient numerical technique for solving the one-dimensional Schrödinger equation for bound states," *Am. J. Phys.* **49**(1), 76–77 (1981).
15. J. Killingbeck, *Microcomputer Algorithms: Action from Algebra*, CRC Press–Taylor and Francis Group, London (1991).
16. J. Stoer and R. Bulirsch, *Introduction to Numerical Analysis, Texts in Applied Mathematics*, Springer, Berlin, Heidelberg (2002).
17. G. T. Einevoll and P. C. Hemmer, "The effective-mass Hamiltonian for abrupt heterostructures," *J. Phys. C: Solid State Phys.* **21**(36), L1193 (1988).
18. K. Young, "Position-dependent effective mass for inhomogeneous semiconductors," *Phys. Rev. B* **39**, 13434–13441 (1989).
19. P. Harrison, *Quantum Wells, Wires and Dots: Theoretical and Computational Physics of Semiconductor Nanostructures*, John Wiley & Sons, Inc., Hoboken, New Jersey (2005).
20. S. F.-P. Paul and H. Fouckhardt, "An improved shooting approach for solving the time-independent Schrödinger equation for III/V QW structures," *Phys. Lett. A* **286**, 199–204 (2001).
21. A. D. Yoffe, "Semiconductor quantum dots and related systems: electronic, optical luminescence and related properties of low dimensional systems," *Adv. Phys.* **50**(1), 1–208 (2001).

22. R. Dingle, *Confined Carrier Quantum States in Ultrathin Semiconductor Heterostructures*, pp. 21–48, Springer, Berlin Heidelberg (1975).
23. K. K. Nanda, F. E. Kruis, and H. Fissan, "Energy levels in embedded semiconductor nanoparticles and nanowires," *Nano Lett.* **1**(11), 605–611 (2001).
24. L. E. Brus, "Electron electron and electron hole interactions in small semiconductor crystallites: the size dependence of the lowest excited electronic state," *J. Chem. Phys.* **80**(9), 4403–4409 (1984).
25. M. Wright and A. Uddin, "Organic-inorganic hybrid solar cells: a comparative review," *Sol. Energy Mater. Sol. Cells* **107**, 87–111 (2012).
26. H. Suzuki, "Electron affinity of semiconducting compound CdSe," *Jpn. J. Appl. Phys.* **5**, 153 (1966).
27. A. Osherov et al., "Tunability of the optical band edge in thin PbS films chemically deposited on GaAs(100)," *J. Phys. Condens. Matter* **22**(26), 262002 (2010).
28. B.-R. Hyun et al., "Electron injection from colloidal PbS quantum dots into titanium dioxide nanoparticles," *ACS Nano* **2**(11), 2206–2212 (2008).
29. R. Dalven, "A review of the semiconductor properties of PbTe, PbSe, PbS and PbO," *Infrared Phys.* **9**(4), 141–184 (1969).
30. Y. Kayanuma, "Quantum-size effects of interacting electrons and holes in semiconductor microcrystals with spherical shape," *Phys. Rev. B* **38**, 9797–9805 (1988).
31. J. Jasieniak et al., "Re-examination of the size-dependent absorption properties of CdSe quantum dots," *J. Phys. Chem. C* **113**(45), 19468–19474 (2009).
32. J. E. B. Katari, V. L. V. Colvin, and A. P. Alivisatos, "X-ray photoelectron spectroscopy of CdSe nanocrystals with applications to studies of the nanocrystal surface," *J. Phys. Chem.* **98**(15), 4109–4117 (1994).
33. C. B. Murray, D. J. Noms, and M. G. Bawendi, "Synthesis and characterization of nearly monodisperse CdE (E = S, Se, Te) semiconductor nanocrystallites," *J. Am. Chem. Soc.* **115**(19), 8706–8715 (1993).
34. W. W. Yu et al., "Experimental determination of the extinction coefficient of CdTe, CdSe, and CdS nanocrystals," *Chem. Mater.* **15**, 2854–2860 (2003).
35. V. N. Soloviev et al., "Molecular limit of a bulk semiconductor: size dependence of the band gap in CdSe cluster molecules," *J. Am. Chem. Soc.* **122**(11), 2673–2674 (2000).
36. X. Peng, J. Wickham, and A. P. Alivisatos, "Kinetics of II-VI and III-V colloidal semiconductor nanocrystal growth: focusing of size distributions," *J. Am. Chem. Soc.* **120**(21), 5343–5344 (1998).
37. A. L. Rogach et al., "Synthesis and characterization of a size series of extremely small thiol-stabilized CdSe nanocrystals," *J. Phys. Chem. B* **103**(16), 3065–3069 (1999).
38. S. N. Inamdar, P. P. Ingole, and S. K. Haram, "Determination of band structure parameters and the quasi-particle gap of CdSe quantum dots by cyclic voltammetry," *ChemPhysChem* **9**(17), 2574–2579 (2008).
39. J. S. Steckel et al., "1.3 μm to 1.55 μm tunable electroluminescence from PbSe quantum dots embedded within an organic device," *Adv. Mater.* **15**(21), 1862–1866 (2003).
40. I. Moreels et al., "Composition and size-dependent extinction coefficient of colloidal PbSe quantum dots," *Chem. Mater.* **19**(25), 6101–6106 (2007).
41. W. Ma et al., "Photovoltaic performance of ultrasmall PbSe quantum dots," *ACS Nano* **5**(10), 8140–8147 (2011).
42. Q. Dai et al., "Size-dependent composition and molar extinction coefficient of PbSe semiconductor nanocrystals," *ACS Nano* **3**(6), 1518–1524 (2009).
43. C. B. Murray et al., "Colloidal synthesis of nanocrystals and nanocrystal superlattices," *IBM J. Res. Dev.* **45**(1), 47–56 (2001).
44. A. Lipovskii et al., "Synthesis and characterization of PbSe quantum dots in phosphate glass," *Appl. Phys. Lett.* **71**(23), 3406 (1997).
45. Y. Liu et al., "Dependence of carrier mobility on nanocrystal size and ligand length in PbSe nanocrystal solids," *Nano Lett.* **10**(5), 1960–1969 (2010).
46. W. W. Yu et al., "Preparation and characterization of monodisperse PbSe semiconductor nanocrystals in a noncoordinating solvent," *Chem. Mater.* **16**(17), 3318–3322 (2004).

47. P. Liljeroth et al., "Density of states measured by scanning-tunneling spectroscopy sheds new light on the optical transitions in PbSe nanocrystals," *Phys. Rev. Lett.* **95**(8), 086801 (2005).
48. D. Segets et al., "Determination of the quantum dot band gap dependence on particle size from optical absorbance and transmission electron microscopy measurements," *ACS Nano* **6**(10), 9021–9032 (2012).
49. X. Jiang et al., "PbSe nanocrystal/conducting polymer solar cells with an infrared response to 2 micron," *J. Mater. Res.* **22**, 2204–2210 (2007).
50. J. J. Choi et al., "PbSe nanocrystal excitonic solar cells," *Nano Lett.* **9**(11), 3749–3755 (2009).
51. M. J. Greaney and R. L. Brutchey, "Ligand engineering in hybrid polymer:nanocrystal solar cells," *Mater. Today* **18**(1), 31–38 (2015).
52. C. Sirtori et al., "Nonparabolicity and a sum rule associated with bound-to-bound and bound-to-continuum intersubband transitions in quantum wells," *Phys. Rev. B* **50**(12), 8663–8674 (1994).
53. S. Birner, "Intersubband transitions in InGaAs/AlInAs multiple quantum well systems," October 2014, http://www.nextnano.com/nextnano3/tutorial/1Dtutorial_InGaAs_MQWs.htm (2015).

François Thierry is a PhD student at the Aix-Marseille University in France. He received his MEng and MSc degrees in material physics and optics and nanotechnology, respectively, from the University of Technology of Troyes in 2012. His current research interests include optoelectronic systems, third-generation solar cells, and confinement effects. He is a student member of SPIE.

Judikaël Le Rouzo is presently an associate professor in physics at Aix-Marseille University, France. He received his PhD in physics from the Ecole Polytechnique, France. His research, done at the IM2NP CNRS laboratory, is centered on optoelectronic devices, such as photodetectors and photovoltaic solar cells. He specializes in optics and photonics. He authored more than 30 publications or conferences in the last five years. He is a reviewer for *Optics Letters* and *Solar Energy Materials and Solar Cells*.

Francois Flory is currently an exceptionnelle class professor at Ecole Centrale Marseille. He is a member of the French Optical Society (SFO), the European Optical Society (EOS), the Optical Society of America (OSA), and SPIE, and a member of the board of editors for the journal *Optik*. His research is mainly in micro/nanostructured optical thin films and optical properties of thin films including quantum dots.

Gerard Berginc received a Dipl. Engineer-Physicist degree from Ecole Centrale de Marseille and his doctorate in theoretical physics. He is currently chief scientist at Thales Optronique. His research activities include fundamental electromagnetic scattering phenomena in ordered and disordered media, coherent effects in random media, localization phenomena, and nano-optics. He has authored over 200 publications in books, journals, and conferences. He holds more than 60 patents. He is a Fellow Member of the Electromagnetics Academy.

Ludovic Escoubas graduated from Centrale Marseille (a French "Grande Ecole" of Engineer), and received a PhD in optics in 1997. He is now professor at Paul Cezanne University (Marseille–France) and leader of the OPTO-PV Team ("Optoelectronics Components and Photovoltaics") of IM2NP (CNRS Laboratory). His current research interests are micro- and nano-optical components and solar cells. He has authored more than 150 papers and communications and holds 6 patents.